Heliyon 9 (2023) e13681

Contents lists available at ScienceDirect

Heliyon

journal homepage: www.cell.com/heliyon

Research article

Clinical implications of hemodynamic analysis for the three-dimension iliac vein model with different stenosis

Xu-Dong Jiang [1], Sheng-Lin Ye [1], Ming Zhang, Xiao-Qiang Li [**], Li-Li Sun [*]

Department of Vascular Surgery, Nanjing Drum Tower Hospital, The Affiliated Hospital of Nanjing University Medical School, Nanjing, Jiangsu, China

ARTICLE INFO

Keywords:
Iliac vein stenosis
Deep venous thrombosis
Hemodynamic
Computational fluid dynamics
Blood stasis

ABSTRACT

Background: The aim of this study was to perform hemodynamic simulations of a three-dimension ideal inferior vena cava-iliac vein model with artificial stenosis to determine the degree of stenosis that requires clinical intervention.

Methods: Four three-dimension stenosis models (30%, 50%, 70%, and 90% stenosis) were constructed using commercial software (Solidworks). The inlet flow rates were acquired from previous literatures to perform the hemodynamic simulations. Changes in the old blood volume fraction, as well conventional hemodynamic parameters including pressure, differential pressure, wall shear stress, and flow patterns, over time were recorded. The pressure at the telecentric region of the stenosis increased with increasing degree of stenosis.

Results: For the 70% stenosis model, the pressure at the telecentric region of the stenosis reached 341 Pa, and the differential pressure between the two ends of the stenosis was 363 Pa (approximately 2.7 mmHg). Moreover, in the 70% and 90% stenosis models, there was a marked change in wall shear stress in the stenosis and the proximal end region, and the flow patterns began to show the phenomenon of flow separation. Blood stasis analysis showed that the 70% stenosis model had the slowest decrease in old blood volume fraction, while the proximal end region had the largest blood residue (15%).

Conclusion: Iliac vein stenosis of approximately 70% is associated with clinically relevant hemodynamic changes, and is more closely related to DVT than other degrees of stenosis.

1. Introduction

Iliac vein stenosis (IVCS) is a disorder of venous return in the lower extremities and pelvis caused by iliac vein compression or abnormal intraluminal adhesions [1]. IVCS is considered the anatomical basis for deep venous thrombosis (DVT) and an important factor for thrombotic recurrence [2,3]. Clinical studies show that after IVCS complicated with DVT, the primary patency rate of

Abbreviations: IVCS, Iliac vein stenosis; DVT, Deep venous thrombosis; CFD, Computational fluid dynamics; PC-MRI, Phase-contrast MR Imaging; IVC, Inferior vena cave; CTV, Computed tomography venography; WSS, Wall shear stress; OBVF, Old blood volume fraction.

* Corresponding author. Department of Vascular Surgery, Nanjing Drum Tower Hospital, The Affiliated Hospital of Nanjing University Medical School, #321 Zhongshan Road, Nanjing, 210008, Jiangsu, China.

** Corresponding author. Department of Vascular Surgery, Nanjing Drum Tower Hospital, The Affiliated Hospital of Nanjing University Medical School, #321 Zhongshan Road, Nanjing, 210008, Jiangsu, China.

E-mail addresses: flytsg@126.com (X.-Q. Li), sunlycn@126.com (L.-L. Sun).

[1] Xu-Dong Jiang and Sheng-Lin Ye contributed equally to this work.

https://doi.org/10.1016/j.heliyon.2023.e13681
Received 30 October 2022; Received in revised form 6 February 2023; Accepted 7 February 2023
Available online 11 February 2023

endovascular treatment is only approximately 57%, which is significantly lower than that of IVCS without DVT [2,4]. Therefore, according to corresponding clinical standards, timely intervention of IVCS in the non-thrombotic period to prevent DVT occurrence will markedly improve patients' quality of life.

There is no consensus on the degree of IVCS that may cause DVT. The current view is that IVCS with moderate or higher stenosis is prone to DVT, although there is no definitive basis for this relationship. The Cardiovascular and Interventional Radiological Society of Europe guidelines for the diagnosis and treatment of IVCS set the degree of stenosis requiring intervention at 30% [5]. Nevertheless, Narayan et al. [6] reported that an IVCS >70% was more prone to lower extremity DVT. Furthermore, Oguzkurt et al. [7] reported that the degree of stenosis in IVCS patients was significantly higher in patients with DVT than those without. However, these findings are mainly based on systematic reviews and analysis of clinical data, without relevant supporting experimental and theoretical studies.

The Virchow's triad includes three categories of factors that can contribute to thrombosis (hypercoagulability, hemodynamic changes [e.g., turbulence or stasis], and endothelial injury/dysfunction). Indeed, in the venous system, blood flow disturbances were reported to cause venous hypertension, leading to DVT formation [8]. The direction of venous blood flow is more prone to thrombosis [9]. Furthermore, Kurstjens et al. [10] reported that preoperative determination of certain hemodynamic parameters for predicting the outcome of deep vein reconstruction in the lower extremities can effectively prevent patients from unnecessary interventions. Thus, the key mechanism underlying various venous diseases, including telangiectasia, varicose veins, and DVT [11–17].

Computational fluid dynamics (CFD), as an emerging experimental tool, can enhance data obtained from CT or MRI by providing a complete representation of hemodynamic simulation under precisely controlled conditions [18]. With the rapid development of computational fluid dynamics (CFD) technology, a number of studies have used CFD to simulate the hemodynamic changes in arteries and veins to assist clinicians in diagnosing diseases and evaluating prognosis [19–24]. Dillon-Murphy et al. [21] used multi-modality image-based computational analysis to simulate the flow of aortic dissection and comparing it with phase-contrast MR Imaging (PC-MRI) data, it was found that large tears had a significant effect on the hemodynamics of the descending and thoracic aorta. López et al. [25] reconstructed the patient specific IVC model based on CTV, and compared the hemodynamic differences of the four IVC filters with CFD, so as to guide the filter selection and the anticoagulant treatment for the patient after the placement of the filter. Wang et al. combined patient CTV and venography to establish an IVC model with renal veins through CFD and found that filter placement above the renal vein opening resulted in increased thrombosis, which is consistent with clinical findings [26]. However, there is no study on the hemodynamic changes of IVCS based on CFD. Thus, in present study, we created an ideal inferior vena cava-IVCS model in combination with a blood stasis model [27–30]. This model was based on a two-fluid principle and was used to determine the timing and location of blood stagnation. The aim of this study was to assess the potential of IVCS to cause DVT, and to determine the relationship between the degree of IVCS and DVT. The models used in this study were constructed based on previous CFD studies in the inferior vena cava [31].

2. Materials and methods

2.1. Model

The normal ideal inferior vena cava-IVCS model used in the present study [32] was constructed using commercial software (Solidworks; Dassault Systemes S.A, Suresnes, France), and included the inferior vena cava and the iliac veins, as shown in Fig. 1(a). To

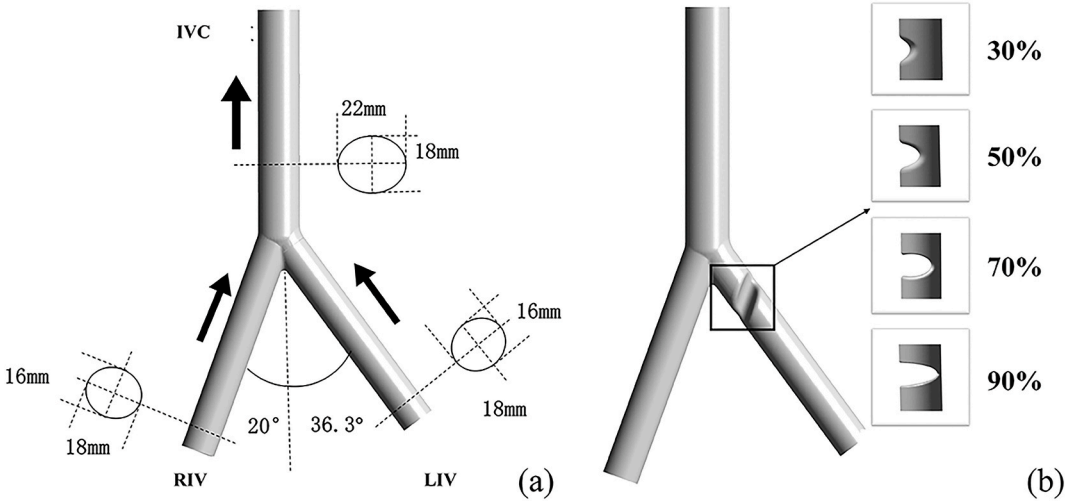

Fig. 1. The ideal inferior vena cava-iliac vein model: a) the normal ideal model, in which the left and right iliac veins are both 50 mm and the inferior vena cava is 100 mm. The left and right iliac veins are ellipses with long and short axes of 18 mm and 16 mm, respectively, and the inferior vena cava is an ellipse with long and short axes of 22 mm and 18 mm, respectively. The angle between the right iliac vein and the centerline of the inferior vena cava is 20°, and the angle between the left iliac vein and the centerline of the inferior vena cava is 36.3°. The black arrow indicates the direction of blood flow; b) the ideal stenosis model with different degrees (30%,50%,70% and 90%).

determine the relationship between the degree of IVCS and DVT, the hemodynamic changes caused by differing degrees of artificial stenosis (established using the normal model) were assessed. According to the definition of the degree of stenosis by Narayan et al. [5, 6], we used stenosis values of 30%, 50%, 70%, and 90%, as shown in Fig. 1(b).

2.2. Mesh

DVT occurring in the iliac vein is generally located around the stenosis. Therefore, we examined both the telecentric and proximal regions of the stenosis for prediction of blood stasis, as shown in Fig. 2. All the inlets and outlets were extended to suppress the computational instability that can occur because of backflow. Unstructured grids were generated using commercial software (Ansys Meshing; Ansys, Inc., Canonsburg, PA, USA). A total of 2.68–2.89 million grids were generated for all stenosis groups using the same setup. Fine boundary layer resolution is essential for guaranteeing accuracy in wall shear stress (WSS) predictions and blood stasis. Thus, five grid layers were added to all venous walls to properly resolve the boundary layer (Fig. 2).

2.3. Numerical simulation

In this study, all CFD simulations were conducted using commercial software (Ansys Fluent Ansys, Inc., Canonsburg, PA, USA). Blood was regarded as an incompressible Newtonian fluid (density of 1055 kg/m^3, dynamic viscosity of 3.5×10^{-3} Pa/s [28–31], while blood flow was assumed to be laminar. The vessel walls were assumed to be rigid with no slip conditions. The blood velocity magnitude was based on previously reported data and the iliac vein blood flow was 2 L/min [32]. In all ideal models, this flow was converted by area into velocity boundary conditions at the inlets of the left and right iliac veins, with a velocity of 0.1474 m/s. At the outlets, the zero-pressure boundary conditions were applied. A novel two-fluid flow model was introduced to simulate the blood stasis [27–30].

3. Results

3.1. Pressure

The pressure gradually decreased from the inlet to the outlet, as shown in Fig. 3. In the absence of stenosis (i.e., in the normal model), the left iliac vein pressure was constant at approximately 35 Pa. In the 30% stenosis model, there was only an increase in pressure in the telecentric stenosis region (by 12.3%). In the 50% stenosis model, the pressure in the telecentric region reached 60 Pa (i.e., 50.3% higher than that at 30% stenosis). When the degree of stenosis reached 70% and 90%, the pressure in the telecentric region reached 341 Pa and 4124 Pa, respectively (4.63 times and 11.1 times higher than at 50% stenosis, respectively). By contrast, the pressure at the proximal stenosis region gradually decreased and approached zero. Overall, these data indicate that the pressure at the telecentric stenosis region increases with increasing degree of stenosis, as does the growth rate, while the pressure downstream of the stenosis gradually decreases with increasing stenosis.

Note that as these were relative pressures do not reflect the actual iliac vein pressure. Thus, to aid with clinical translation, we calculated the differential pressures using a cross-section of the left iliac vein from the telecentric end to the proximal end regions. Two differential pressures were collected—one was the venous differential pressure at both ends of the stenosis, and the other was the left iliac inlet and the interface between the telecentric region and the stenosis region, as shown in Fig. 4(a). It could be obtained from

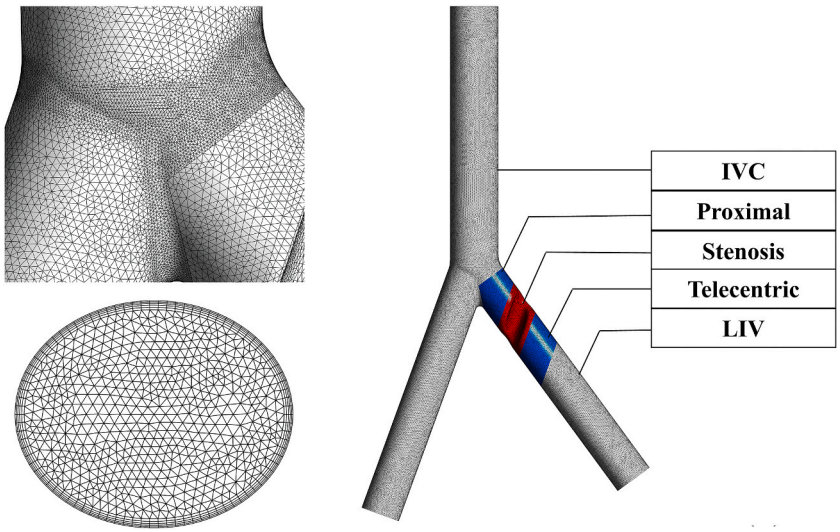

Fig. 2. Computational domain mesh of 50% stenosis degree model, showing domain division, local details and 5 prism layers grids at inlet.

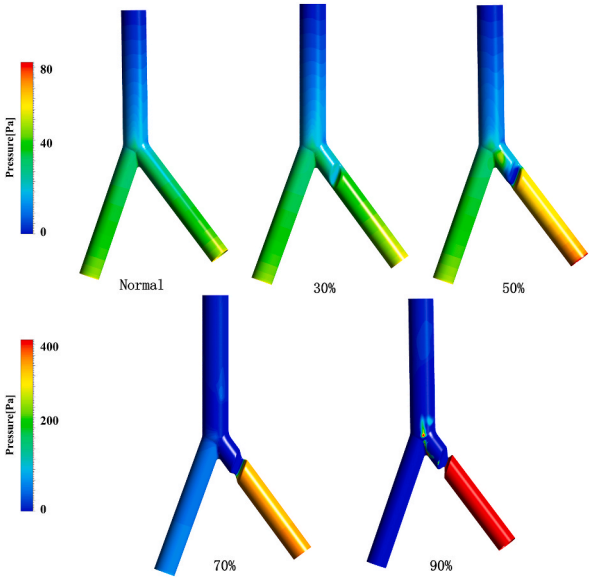

Fig. 3. Pressure contours. The pressure at the telecentric stenosis region increases with increasing degree of stenosis, as does the growth rate, while the pressure downstream of the stenosis gradually decreases with increasing stenosis. The numbers (30%,50%,70% and 90%) under each contours represent different degrees of stenosis, and normal mean no degree of stenosis. Note the 70% and 90% models in the second row, due to the high pressure, a different scale was used to highlight the pressure distribution from the first row. In the 30% stenosis model, there was only an increase in pressure in the telecentric stenosis region (by 12.3%). In the 50% stenosis model, the pressure in the telecentric region reached 60 Pa (i.e., 50.3% higher than that at 30% stenosis). When the degree of stenosis reached 70% and 90%, the pressure in the telecentric region reached 341 Pa and 4124 Pa, respectively (4.63 times and 11.1 times higher than at 50% stenosis, respectively).

Fig. 4(b) that, the differential pressures 1 and 2 both increased with increasing degree of stenosis, while the increase in differential pressure 1 was greater than that of differential pressure 2. In the normal model and the 30% and 50% stenosis models, differential pressures 1 and 2 were both <40 Pa (equivalent to 0.3 mmHg)—c.f. the normal human central venous pressure of 6–12 mmHg and lower extremity venous pressure of 14 mmHg [33]. For the 70% stenosis model, the differential pressure between the two ends of the stenosis was 363 Pa (approximately 2.7 mmHg), which was of clinical relevance, while the deep venous pressure of the lower extremities increased by approximately 1.7 mmHg. When the degree of stenosis reached 90%, the differential pressure further increased to >30 mmHg.

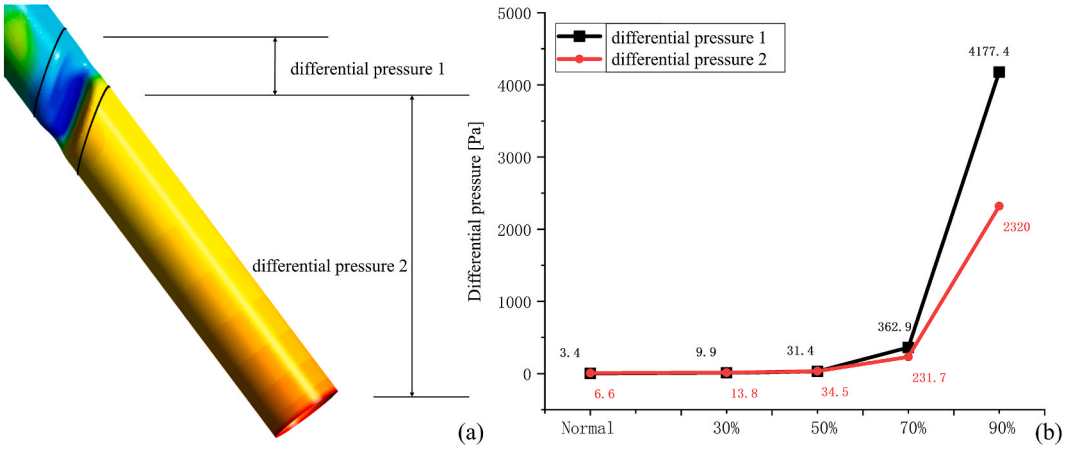

Fig. 4. Differential pressure in ideal stenosis model: a) the segment corresponding to differential pressure 1 and differential pressure 2, differential pressure 1 was the pressure difference between the two ends of the stenosis, and differential pressure 2 was the pressure difference of the deep veins of the lower extremities; b) comparison of the differential pressure value. the differential pressures 1 and 2 both increased with increasing degree of stenosis, while the increase in differential pressure 1 was greater than that of differential pressure 2. In the normal model and the 30% and 50% stenosis models, differential pressures 1 and 2 were both <40 Pa (equivalent to 0.3 mmHg)—c.f. the normal human central venous pressure of 6–12 mmHg and lower extremity venous pressure of 14 mmHg [33]. For the 70% stenosis model, the differential pressure between the two ends of the stenosis was 363 Pa (approximately 2.7 mmHg), which was of clinical relevance, while the deep venous pressure of the lower extremities increased by approximately 1.7 mmHg. When the degree of stenosis reached 90%, the differential pressure further increased to >30 mmHg.

3.2. WSS

The WSS of the normal iliac vein segment only increased slightly at the junction with the inferior vena cava, as shown in Fig. 5. In the stenosis model, the WSS at the stenosis was markedly larger than the rest of the vessel (indicated by the arrow in the red area). In the 50% stenosis model, the WSS at the proximal end region increased significantly, while the proportion of red regions also increased. By contrast, there was no change in the WSS of the telecentric region. In the 70% stenosis model, the WSS of the inferior vena cava markedly increased—this was predominantly in the right and anterior walls, which may be related to the rapid jet of the left iliac vein caused by the stenosis.

The area-averaged WSS of each computational domain was shown in Fig. 6(a–b). With increasing degree of stenosis, there was an increase in the WSS of the stenosis region and the proximal end region (this was greatest at the stenotic region). In the 30% stenosis model, the increase in WSS remained within the normal range of the vein (the WSS values of the proximal end and the stenosis were 0.54 Pa and 0.72 Pa, respectively). In the 50% stenosis model, the WSS at the proximal end region and the stenosis area increased beyond the normal physiological range (>1 Pa). In the 70% stenosis model, the WSS showed more marked changes, with values of 2.28 Pa and 4.60 Pa in the proximal end region and the stenosis, respectively (1 and 2 times higher than that of the 50% model, respectively). Finally, in the 90% stenosis model, the WSS changes were even greater, with an increase of >3 times compared with the changes in the 70% model, far exceeding the normal physiological value. Note that there were no changes in the WSS at the telecentric end regions between the groups, with WSS values remaining stable at approximately 0.54 Pa.

3.3. Flow patterns

Analysis of the flow patterns of each stenosis model showed that stenosis only affected the downstream flow field, but not the upstream flow (i.e., the telecentric end of the stenosis). With increasing degree of stenosis, there was a significant gradual increase in flow velocity at the stenosis entrance and the proximal end region. In the 30% stenosis model, there was only a minor change in flow velocity at the stenosis and proximal end region compared with that in the normal model (0.146 m/s and 0.153 m/s, respectively), with similar flow velocities to the inlet of the left iliac vein. In the 50% and 90% stenosis models, the flow velocity at the stenosis and proximal end region increased significantly—velocity at the stenosis increased from 0.199 m/s in the 50% stenosis model to 0.665 m/s in the 90% stenosis model, while velocity at the proximal end region increased from 0.161 m/s in the 50% stenosis model to 0.442 m/s in the 90% stenosis model.

In the normal model, the flow pattern of the left iliac vein was stable and similar to that of the right iliac vein, as shown in Fig. 7. However, in the stenosis models, the flow velocity at the stenosis regions increased and affected the flow field in the inferior vena cava. Furthermore, downstream of the stenosis, the increased flow velocity causes a decrease in the pressure intensity at the proximal end region, and the blood flowed back into the proximal end from the right iliac vein. This resulted in the phenomenon of flow separation, with formation of a secondary flow and a local blood flow disorder. In the 70% stenosis model, the high-velocity blood flow had a

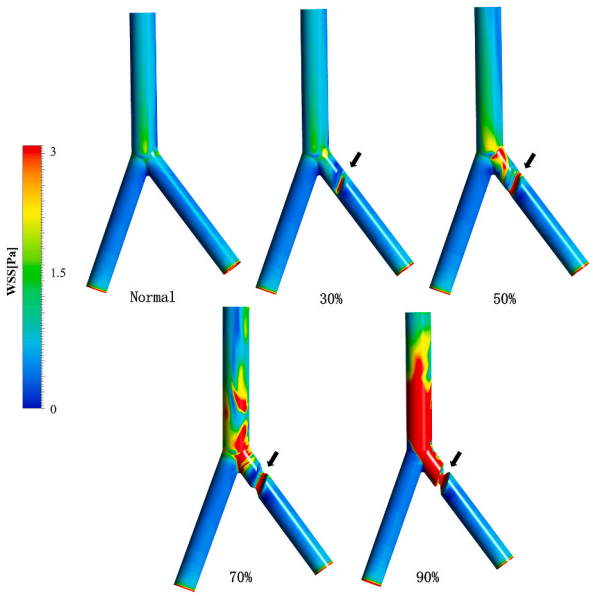

Fig. 5. Wall shear stress (WSS) contours, the blue part represented the low WSS area, and the red part represented the high WSS area. As indicated by the arrow, the WSS increased significantly at the stenosis regions. The numbers (30%,50%,70% and 90%) under each contours represent different degrees of stenosis, and normal mean no degree of stenosis. (For interpretation of the references to colour in this figure legend, the reader is referred to the Web version of this article.)

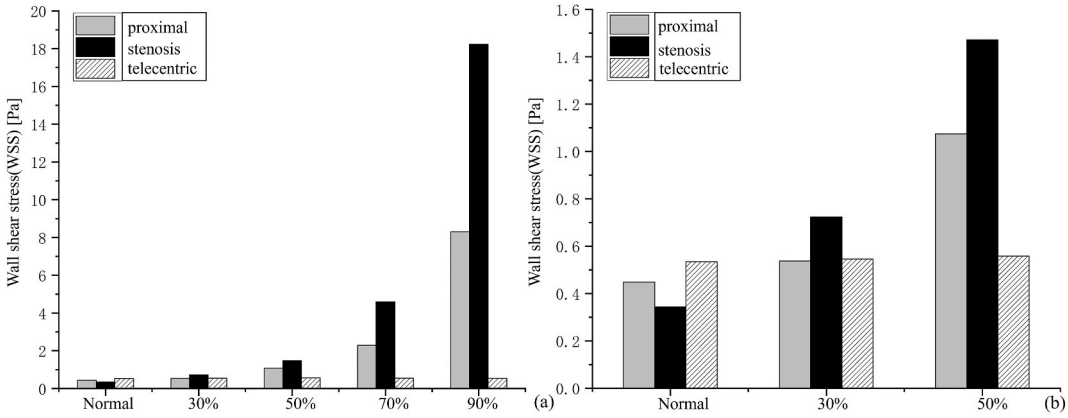

Fig. 6. Wall shear stress (WSS) value: a) with increasing degree of stenosis, there was an increase in the WSS of the stenosis region and the proximal end region (this was greatest at the stenotic region), while there were no changes in the WSS at the telecentric end regions between the groups, with WSS values remaining stable at approximately 0.54 Pa. In the 50% stenosis model, the WSS at the proximal end region and the stenosis area increased beyond the normal physiological range (>1 Pa). In the 70% stenosis model, the WSS showed more marked changes, with values of 2.28 Pa and 4.60 Pa in the proximal end region and the stenosis, respectively (1 and 2 times higher than that of the 50% model, respectively); b) due to the low WSS values of the normal, 30% and 50% models, the difference was not obvious in Figure a, so the Figure b used different scales to highlight the difference.

marked impact on the streamlines of the inferior vena cava. Furthermore, the 90% stenosis model showed the greatest disturbance in inferior vena cava blood flow, and a small vortex appeared at the junction with the left iliac vein.

3.4. Blood stasis

Prediction results of the blood stasis model showed no evidence of blood stasis. In all models, the old blood volume fraction (OBVF) decreased gradually over time. At the telecentric end region, the OBVF eventually approached 0, indicating that the blood had not stagnated. In the normal model, the OBVF decreased most rapidly, with the OBVF at the stenosis and the proximal end region approaching 0 at 1.5 s and 1.7s, respectively. In the 30% stenosis model, although the decrease in OBVF was not as marked as that in the normal model, there was no residual blood in the proximal end region or the stenosis.

To compare the OBVF at the stenosis and proximal end region between the different models, the time course of changes in OBVF was assessed, as shown in Fig. 8(a and b). Blood began to stagnate at the proximal end region in the 50% stenosis model, with the OBVF maintained at approximately 13% from 2.3s. In the 70% stenosis model, the proximal end region OBVF was maintained at approximately 15% from 2.5 s. However, the proximal end region OBVF decreased in the 90% stenosis model, and remained at approximately 6% from 2.2 s. Blood stasis at the stenosis was less obvious than that at the proximal end region. In the 50% stenosis model, the OBVF remained at approximately 5% from 1.8 s, but approached 0 after the simulation converged in all other models. Note that the OBVF in the stenosis and proximal end region decreased most slowly in the 70% model, indicating the highest blood stasis. In the 90% stenosis

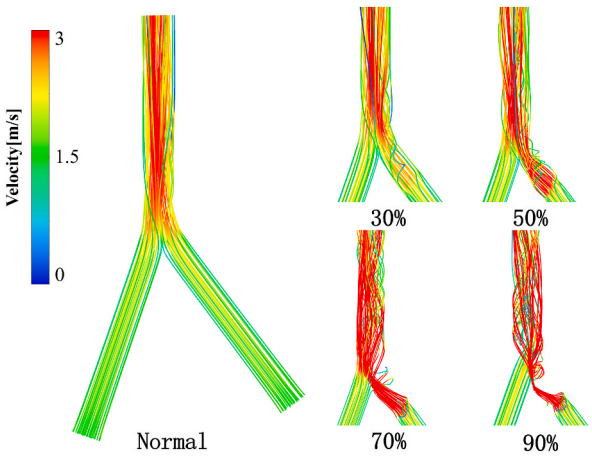

Fig. 7. Flow patterns (As the stenosis degree increased, the flow field at the stenosis and downstream was gradually disordered). The numbers (30%,50%,70% and 90%) under each contours represent different degrees of stenosis, and normal mean no degree of stenosis.

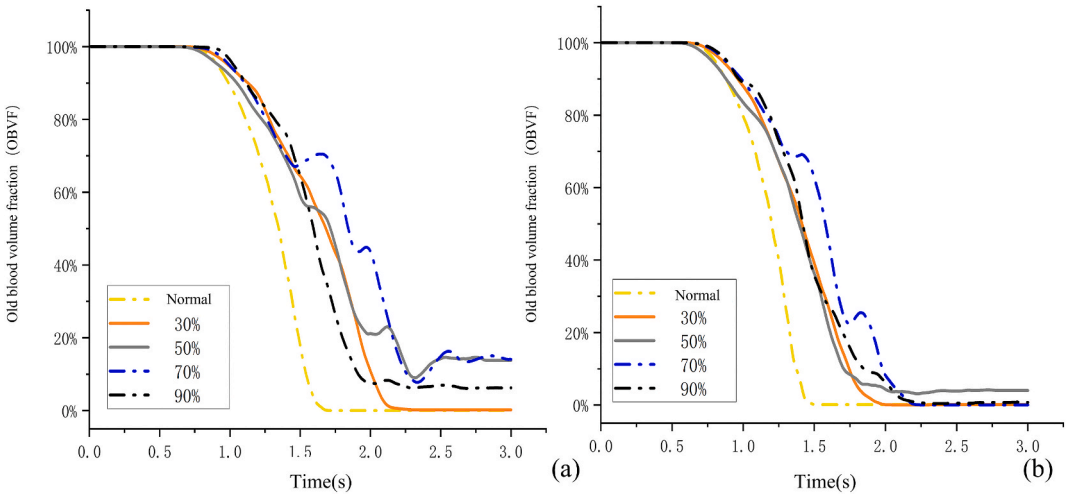

Fig. 8. The time histories of OBVF: a) the proximal end OBVF; b) the stenosis region OBVF.

model, the decrease in OBVF at the proximal end region was faster than that in the 50% model, indicating that excessive stenosis was not conducive to blood stasis.

4. Discussion

The present study examined the effects of IVCS on blood vessel pressure, WSS, flow patterns, and OBVF using numerical simulation of ideal stenosis models. The use of artificial blood vessel models to study the hemodynamics of various diseases has been reported for the coronary arteries and the inferior vena cava [31,33–35], including for stenosis models [36]. As shown in Fig. 3, the pressure at the telecentric end of stenosis was significantly higher than that at the proximal region, and the pressure increased with the increase of stenosis degree, which was similar to results of Liu et al. [36]. In the study of Singer et al. [34] and Wang et al. [26] on inferior vena cava filter, whether WSS greater than 2Pa was considered to determine whether thrombosis occurred. In our study, as shown in Figs. 5 and 6, WSS at the stenosis area increased significantly, and when the stenosis degree was greater than 70%, WSS at the stenosis and proximal end began to be greater than 2Pa, indicating that 70% stenosis degree was closely related to DVT. However, these studies only used traditional hemodynamic parameters. In the present study, a blood stasis model created by our research group was adopted to simulate the situation of blood stasis. As shown in Fig. 7, beginning from the model with 50% stenosis degree, there were different degrees of blood retention in both the stenosis and the proximal end of the stenosis, which was consistent with the results of another study on IVCS patients with collaterals. In that study, the degree of blood stasis on stenosis was significantly higher than our study [27], which may be related to blood flow disturbance caused by collaterals. We found that stenosis changed blood flow within and downstream of the stenosis, and also affected flow of the inferior vena cava and the contralateral iliac vein. Furthermore, the severity of changes in the various hemodynamic parameters increased with increasing degree of stenosis. In the blood stasis analysis, only the 50% and 70% stenosis models showed any evidence of blood stasis in the stenosis and the proximal end region. Nevertheless, the OBVF did not exceed 20%, indicating minimal effects of simple stenosis on blood stasis.

Clinically, IVCS is diagnosed by measuring the venous pressure difference. In general, a differential pressure between the two ends of the stenosis >2 mmHg is considered to reflect IVCS with clinical manifestations, and is associated with DVT [33]. In addition, Imaging data such as CTV can also assist the diagnosis and treatment of IVCS patients with DVT, Narayan et al. [6] performed a case-control study in a cohort of 230 IVCS patients with a diagnosis of unilateral DVT based on their CTV data, and the results showed that greater than 70% compression may be associated with left DVT. In the present study, the 70% stenosis model showed a pressure difference between the two ends of the stenosis >2 mmHg (2.7 mmHg). Moreover, this model showed a marked change in the corresponding position, and the flow field began to show the phenomenon of flow separation. We also found that the 70% stenosis model had the slowest decline in OBVF, and the proximal end region showed the largest blood residue (15%). On the basis of these data and the previous case review, we suggest that clinical manifestations such as lower extremity venous hypertension will appear when the degree of IVCS reaches 70%, with a stronger correlation with DVT. Note that the 50% stenosis model showed no clinically relevant hemodynamic changes using traditional hemodynamic parameters such as pressure and WSS. Nevertheless, this model showed residual blood in both the stenosis and the proximal end region, with OBVF values of 6% and 13%, respectively. Thus, IVCS values of approximately 50% should also be considered important. By contrast, the hemodynamic parameters of the 30% stenosis model were within the range of the normal model, suggesting that an IVCS of 30% has no obvious clinical significance. Finally, although the hemodynamic parameters in the 90% stenosis model were much higher than normal values, in clinical practice, most patients with 90% stenosis have occlusion of the iliac vein segment.

This study also has some limitations. First, similar to the previous study [26,31,34], the outlet pressure was set as zero, which may affect the accuracy of the results. Second, the wall was set to be rigid, which may not be consistent with the high venous compliance

[37]. Finally, there was no obvious effect of simple stenosis on the degree of blood stasis. Even so, DVT due to IVCS can occur at the stenosis, proximal end, and the telecentric end. However, we found no significant effect stenosis on hemodynamic parameters in the upstream region (telecentric end) of the stenosis.

5. Conclusion

In this study, based on the simulation results and the previous literature review our data, it suggests that an IVCS of approximately 70% is associated with clinically relevant hemodynamic changes, and is most closely related to DVT compared with other degrees of stenosis. Nevertheless, other factors may also contribute to the relationship between IVCS and DVT. Thus, further studies are required to examine more complex hemodynamic changes caused by other pathological structures such as collateral circulation.

Author contribution statement

Xu-Dong Jiang, Sheng-Lin Ye: Conceived and designed the experiments; Performed the experiments; Analyzed and interpreted the data; Wrote the paper. Ming Zhang: Analyzed and interpreted the data; Contributed reagents, materials, analysis tools or data. Xiao-Qiang Li, Li–Li Sun: Conceived and designed the experiments; Performed the experiments; Analyzed and interpreted the data; Wrote the paper.

Funding statement

This work was supported by National Natural Science Foundation of China [No. 82070496].

Data availability statement

No data was used for the research described in the article.

Declaration of competing interest

The authors declare no conflict of interest.

References

[1] M.R. Kim, et al., Deep venous thrombosis caused by iliac vein compression syndrome, Ann. Emerg. Med. 44 (4) (2004).
[2] Q.Y. Meng, et al., Endovascular treatment of iliac vein compression syndrome, Chin Med J (Engl) 124 (20) (2011) 3281–3284.
[3] S. Vedantham, et al., Quality improvement guidelines for the treatment of lower-extremity deep vein thrombosis with use of endovascular thrombus removal, J. Vasc. Intervent. Radiol. 25 (9) (2014) 1317–1325.
[4] Q.Y. Meng, et al., Stenting of iliac vein obstruction following catheter-directed thrombolysis in lower extremity deep vein thrombosis, Chin Med J (Engl) 126 (18) (2013) 3519–3522.
[5] A.H. Mahnken, et al., CIRSE standards of practice guidelines on iliocaval stenting, Cardiovasc. Intervent. Radiol. 37 (4) (2014) 889–897.
[6] A. Narayan, et al., Iliac vein compression as risk factor for left-versus right-sided deep venous thrombosis: case-control study, Radiology 265 (3) (2012) 949–957.
[7] L. Oguzkurt, et al., Compression of the left common iliac vein in asymptomatic subjects and patients with left iliofemoral deep vein thrombosis, J. Vasc. Intervent. Radiol. 19 (3) (2008) 366–370. ; quiz 371.
[8] J.J. Chiu, S. Chien, Effects of disturbed flow on vascular endothelium: pathophysiological basis and clinical perspectives, Physiol. Rev. 91 (1) (2011) 327–387.
[9] A.S. Wolberg, et al., Procoagulant activity in hemostasis and thrombosis: virchow's triad revisited, Anesth. Analg. 114 (2) (2012) 275–285.
[10] R. Kurstjens, et al., The predictive value of haemodynamic parameters for outcome of deep venous reconstructions in patients with chronic deep vein obstruction - a systematic review, Phlebology 32 (8) (2017) 532–542.
[11] Y.S. Li, J.H. Haga, S. Chien, Molecular basis of the effects of shear stress on vascular endothelial cells, J. Biomech. 38 (10) (2005) 1949–1971.
[12] R.M. Nerem, et al., The study of the influence of flow on vascular endothelial biology, Am. J. Med. Sci. 316 (3) (1998) 169–175.
[13] Q. Ji, et al., Short-term effects of double-layer autologous vein graft on restraint of excessive distension and alleviation of neointimal hyperplasia in a porcine saphenous vein graft model, Heart Ves. 26 (2) (2011) 190–195.
[14] K. Mavromatis, et al., Early effects of arterial hemodynamic conditions on human saphenous veins perfused ex vivo, Arterioscler. Thromb. Vasc. Biol. 20 (8) (2000) 1889–1895.
[15] J.J. Wentzel, et al., Endothelial shear stress in the evolution of coronary atherosclerotic plaque and vascular remodelling: current understanding and remaining questions, Cardiovasc. Res. 96 (2) (2012) 234–243.
[16] U. Morbiducci, et al., Blood damage safety of prosthetic heart valves. Shear-induced platelet activation and local flow dynamics: a fluid-structure interaction approach, J. Biomech. 42 (12) (2009) 1952–1960.
[17] S. Einav, D. Bluestein, Dynamics of blood flow and platelet transport in pathological vessels, Ann. N. Y. Acad. Sci. 1015 (2004) 351–366.
[18] Z. Sun, Coronary CT angiography: beyond morphological stenosis analysis, World J. Cardiol. 5 (12) (2013) 444–452.
[19] J.F. LaDisa, et al., Stent design properties and deployment ratio influence indexes of wall shear stress: a three-dimensional computational fluid dynamics investigation within a normal artery, J. Appl. Physiol. 97 (1) (2004) 424–430.
[20] H. Xu, et al., Coupled morphological-hemodynamic computational analysis of type B aortic dissection: a longitudinal study, Ann. Biomed. Eng. 46 (7) (2018) 927–939.
[21] D. Dillon-Murphy, et al., Multi-modality image-based computational analysis of haemodynamics in aortic dissection, Biomech. Model. Mechanobiol. 15 (4) (2016) 857–876.
[22] G. Garcia-Isla, et al., Sensitivity analysis of geometrical parameters to study haemodynamics and thrombus formation in the left atrial appendage, Int J Numer Method Biomed Eng (2018) e3100.
[23] G.M. Bosi, et al., Computational fluid dynamic analysis of the left atrial appendage to predict thrombosis risk, Front Cardiovasc Med 5 (2018) 34.
[24] E. Georgakarakos, et al., The influence of intraluminal thrombus on abdominal aortic aneurysm wall stress, Int. Angiol. 28 (4) (2009) 325–333.
[25] J.M. Lopez, et al., A comparative CFD study of four inferior vena cava filters, Int J Numer Method Biomed Eng 34 (7) (2018) e2990.

[26] S.L. Wang, M.A. Singer, Toward an optimal position for inferior vena cava filters: computational modeling of the impact of renal vein inflow with Celect and TrapEase filters, J. Vasc. Intervent. Radiol. 21 (3) (2010) 367–374. ; quiz 374.
[27] X. Jiang, et al., Patient-specific hemodynamic analysis of IVCS-induced DVT, Comput. Methods Biomech. Biomed. Eng. 25 (11) (2022) 1211–1221.
[28] X. Jiang, et al., A two-fluid blood stasis model for false lumen thrombosis after type B dissection repair, Comput. Methods Biomech. Biomed. Eng. 25 (13) (2022) 1499–1508.
[29] W.F. Dai, P. Wu, G.M. Liu, A two-phase flow approach for modeling blood stasis and estimating the thrombosis potential of a ventricular assist device, Int. J. Artif. Organs 44 (7) (2021) 471–480.
[30] X. Jiang, et al., A hemodynamic analysis of the thrombosis within occluded coronary arterial fistulas with terminal aneurysms using a blood stasis model, Front. Physiol. 13 (2022), 906502.
[31] E. Rahbar, D. Mori, J.E. Moore Jr., Three-dimensional analysis of flow disturbances caused by clots in inferior vena cava filters, J. Vasc. Intervent. Radiol. 22 (6) (2011) 835–842.
[32] B.A. Craven, K.I. Aycock, K.B. Manning, Steady flow in a patient-averaged inferior vena cava-Part II: computational fluid dynamics verification and validation, Cardiovasc Eng Technol 9 (4) (2018) 654–673.
[33] Z. Liu, et al., Endovascular treatment for symptomatic iliac vein compression syndrome: a prospective consecutive series of 48 patients, Ann. Vasc. Surg. 28 (3) (2014) 695–704.
[34] M.A. Singer, W.D. Henshaw, S.L. Wang, Computational modeling of blood flow in the TrapEase inferior vena cava filter, J. Vasc. Intervent. Radiol. 20 (6) (2009) 799–805.
[35] D.G. Katritsis, et al., Flow patterns at stented coronary bifurcations: computational fluid dynamics analysis, Circ Cardiovasc Interv 5 (4) (2012) 530–539.
[36] J. Liu, F. Yu, Y. Zhang, Flow resistance coefficient analysis of left anterior descending artery stenosis: a preliminary study, Proc. Inst. Mech. Eng. H 234 (1) (2020) 100–109.
[37] E. Tedaldi, et al., An experimental and computational study of the inferior vena cava hemodynamics under respiratory-induced collapse of the infrarenal IVC, Med. Eng. Phys. 54 (2018) 44–55.